ISIJ International, Vol. 62 (2022), No. 11, pp. 2402–2409
https://doi.org/10.2355/isijinternational.ISIJINT-2022-311

Hydrogen Effect on the Mobility of Edge Dislocation in α-Iron: A Long-Timescale Molecular Dynamics Simulation

Ryosuke MATSUMOTO,[1)]* Sunday T. OYINBO,[2)] Mugilgeethan VIJENDRAN[3)] and Shinya TAKETOMI[4)]

1) Department of Mechanical and Electrical Systems Engineering, Kyoto University of Advanced Science, 18, Yamanouchi-Gotandacho, Ukyo-word, Kyoto, 615-8577 Japan.
2) Nagamori Institute of Actuators, Kyoto University of Advanced Science, 18, Yamanouchi-Gotandacho, Ukyo-word, Kyoto, 615-8577 Japan.
3) Graduate Student, Department of Mechanical and Electrical Systems Engineering, Kyoto University of Advanced Science, 18, Yamanouchi-Gotandacho, Ukyo-word, Kyoto, 615-8577 Japan.
4) Department of Mechanical Engineering, Saga University, 1 Honjo-machi, Saga, 840-8502 Japan.

(*Received on June 30, 2022; accepted on August 3, 2022; J-STAGE Advance published date: August 23, 2022*)

Explaining the hydrogen effect on dislocation mobility is crucial to revealing the mechanisms of hydrogen-related fracture phenomena. According to the general perspective, reducing the speed of dislocation can give enough time to hydrogen to catch up with the dislocation migration. In this research, we conducted molecular dynamics (MD) simulations to investigate the impact of hydrogen on the edge-dislocation motion in α-iron at various dislocation speeds and temperatures. It was discovered that, for all hydrogen concentrations evaluated in this paper, the hydrogen effect on dislocation transition from pinning to dragging occurs at a dislocation speed of around 0.1 m/s at 300 K. When the dislocation velocity is reduced to 0.01 m/s employing long timescale MD simulations over 1 μs, it is observed that hydrogen follows dislocation motion with small jumps in the dislocation core. The required stress to migrate the edge dislocation at a speed of 0.01 m/s was discovered to be 400 MPa, even at a lower hydrogen concentration, which was achieved in a gaseous hydrogen environment with lower pressure than atmospheric pressure. Although the dislocation still traps hydrogen at 500 K, as temperature increases, the impact of hydrogen on the shear stress required for dislocation glide becomes negligibly small. The required shear stress at lower dislocation speeds was predicted by employing the stress-dependent thermal activation model assuming the hydrogen diffusion rate-determining. The finding demonstrated that the edge dislocation should slow down until 1 mm/s order or less in the presence of hydrogen and suitable stress for α-iron.

KEY WORDS: edge dislocation; molecular dynamics; iron; dislocation; hydrogen; mobility.

1. Introduction

The mechanical properties of different metallic materials are degraded by hydrogen. Understanding the process of hydrogen embrittlement is crucial to predicting the materials' reliability under hydrogen environments and developing hydrogen-resistant materials. Numerous mechanisms of hydrogen embrittlement include Hydrogen Enhanced Localized Plasticity (HELP),[1)] Hydrogen Enhanced DEcohesion (HEDE),[2)] Hydrogen Enhanced Strain-Induced Vacancy (HESIV),[3)] and more[4)] have been proposed. The hydrogen effect on dislocation mobility has long been a central question of microscopic hydrogen effect, attracting researchers and engineers in the related fields, since dislocation mobility more or less affects all mechanisms.

When hydrogen gas was introduced, the dislocations were observed to migrate or accelerate under the observation by Transmission Electron Microscope (TEM) for different materials including α-iron.[5)] First, the phenomenon was explained by an elastic shielding effect because of hydrogen accumulation and reduction of elastic constants employing the Finite Element Method (FEM) analysis.[6)] However, it has become known that the explanation is only valid for some materials where the hydrogen concentration can be extremely high around dislocations. In contrast, the macroscopic stress-strain curves tend to exhibit hardening in the presence of hydrogen in many cases.[7)]

For its distribution to be experimentally directly measured, the amount of hydrogen that can be dissolved in α-iron is too minute. Thus, atomistic simulations and Density Functional Theory (DFT) computations are potent tools to demonstrate the hydrogen effect, and therefore they

* Corresponding author: E-mail: matsumoto.ryosuke@kuas.ac.jp

have been used in numerous investigations. For example, the hydrogen effect on the mobility of screw and edge dislocations was examined by employing static computations including the Nudged Elastic Band (NEB) method,[8] and it was demonstrated that depending on the hydrogen concentration, applied shear stress, and temperature in α-iron, hydrogen can either improve or decrease dislocation velocity.[9–11] The pioneering MD simulation demonstrated that hydrogen hinders edge dislocation motion.[12] Recently, it was asserted that the improved plasticity is generated by hydrogen trapped locally in the dislocation cores.[13] The author proposed that the adsorption and desorption of hydrogen on materials surfaces result in a change in apparent surface energy, which can lead to dislocation migration in thin films.[14] After all, although intensive investigations have been conducted, the hydrogen effect on dislocation mobility has not been clarified yet.

This research employs MD simulations, including long-timescale simulations over 1 μs, to study the hydrogen effect on the edge-dislocation mobility and migration behavior at a wide range of dislocation speeds in α-iron. The MD simulations enable direct evaluation of the thermal fluctuation effects on dislocation and hydrogen motion, and it can automatically find the minimum energy path for the reaction at given calculation conditions.

2. Methodology

The in-house program for MD simulation that was employed previously in various computations[15,16] was used in this research. The Embedded Atom Method (EAM) potential developed by M. Wen[17] was employed. The EAM potential can adequately reproduce the heat of solution of hydrogen under shear stress,[18] the migration energy of hydrogen,[15] and the interaction energy between hydrogen atom and various lattice defects in α-iron.[19–21] Although the accuracy for screw dislocation structure and surface energies are not good, this paper does not treat them.

Time steps of Δt = 2 fs and Δt/24 fs were respectively used for Fe and H atoms by employing the reversible Reference System Propagator Algorithms (rRESPA).[22] The simulation model is the same as the previous investigate;[16] α-iron single crystal contains 8 230 Fe atoms with dimensions of L_x = 11.07 nm, L_y = 4.22 nm, and L_z = 2.03 nm along x-, y- and z-directions with [111], [$\bar{1}\bar{1}$2], and [1$\bar{1}$0], respectively [**Fig. 1**(a)]. The Periodic boundary conditions (PBC) were used in the x and z axes, and the ($\bar{1}\bar{1}$2)[111] edge dislocation was added at the unit cell's center. The upper and lower three atomic layers were fixed in the y-direction, and the relaxation was carefully conducted under an intended constant temperature (T = 300 K, 400 K, or 500 K) for a total of 20 ps.

Then hydrogen atoms are added to the sites with the highest and the second highest trap energy,[23] which periodically exists along with the dislocation core. The hydrogen concentration is C_H = 0.5 nm^{-1} (one H atom), 1 nm^{-1} (two H atoms), 2.5 nm^{-1} (five H atoms), and 5 nm^{-1} (ten H atoms) along the dislocation line. The corresponding hydrogen gas pressure, which represents these hydrogen concentrations at thermal equilibrium at 300 K, is lower than atmospheric pressure[11] even for the highest hydrogen concentration in this study. Then relaxation was conducted again after introducing H atoms for 200 ps. If a hydrogen atom enteres the upper or lower fixed boundary region after diffusion, the velocity along the hydrogen atom's y-direction is reversed. Therefore, all hydrogen atoms are kept in the middle of the simulation model throughout the computation. The hydrogen distribution after the relaxation for C_H = 5 nm^{-1} (ten H atoms) and T = 300 K is demonstrate in Figs. 1(b) and 1(c). All hydrogen atoms are trapped in the dislocation core.

The velocity along the x-direction of atoms in the upper and lower boundary regions was controlled to enforce the intended dislocation velocities (V_d = 10 m/s, 1 m/s, 0.1 m/s, and 0.01 m/s). The dislocation travels L_x when the relative displacement of the upper boundary to the lower boundary is b, where b represents the length of Burgers vector. The temperature was kept constant during the simulation. The computation was conducted until the dislocation returned to the original position through the PBC in the x-direction except for some conditions including T = 500 K. The calculation conditions are surmmarized in **Table 1**.

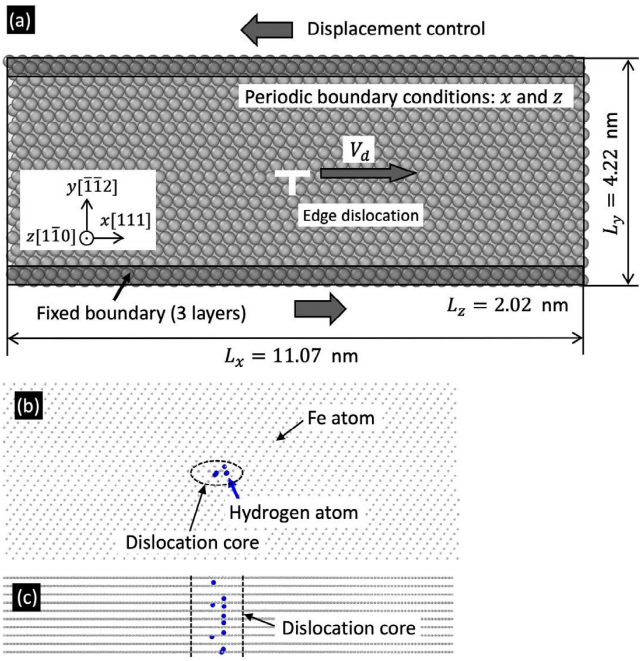

Fig. 1. A simulation model with edge dislocation: (a) demonstrates the overall structure, and (b) and (c) demonstrate the hydrogen distributions after relaxation for C_H = 5 nm^{-1} (ten H atoms) and T = 300 K. (b) and (c) demonstrate the views from z- and y-direction respectively. Small gray dots and large blue dots are Fe and H atoms, respectively. (Online version in color.)

Table 1. Calculation conditions for MD simulations.

Parameters	Values
Model size $L_x \times L_y \times L_z$ [nm^3] at 0 K	11.05 × 4.91 × 2.02
Duration of simulation	1.1 ns–1.1 μs
Timestep [fs]	2 fs for Fe and 2/24 fs for H
Dislocation velocity V_d [m/s]	10, 1, 0.1, and 0.01
Temperature T [K]	Constant at 300, 400, and 500
Hydrogen concentration C_H [nm^{-1}]	0.5, 1, 2.5, and 5

3. Results and Discussion

3.1. Hydrogen Effect at a Higher-Speed Migration

Figure 2 demonstrates the shear stress (τ_{xy}) evolution at higher dislocation speeds (V_d = 10 and 1 m/s) at T = 300 K. The shear-stress curves have a prominent peak at first (1–4 ns for V_d = 1 m/s), then rapidly reduce to nearly zero. The difference between V_d = 10 and 1 m/s was small. There are fluctuations in shear stress at the end of the computation, as demonstrated in Fig. 2 (8–11 ns for V_d = 1 m/s). This is because the dislocation returns to the original position through the periodic boundary, and then the dislocation interacts with hydrogen atoms, which stay near the initial position.

Figure 3 demonstrates how hydrogen diffuses during dislocation migration where V_d = 1 m/s and T = 300 K. The structure analysis was conducted employing common neighbor analysis (CNA)[24] integrated into OVITO.[25] Figure 3(a) demonstrates the structure change for the highest hydrogen concentration (C_H = 5 nm^{-1}). Initially, all hydrogen atoms exist in the dislocation core [Fig. 3(a)(1)]. When the dislocation gradually moves, the hydrogen atoms exist at the tail of the dislocation core [Fig. 3(a)(2)]. This period closely corresponds to the peak stress in Fig. 2. Then, only

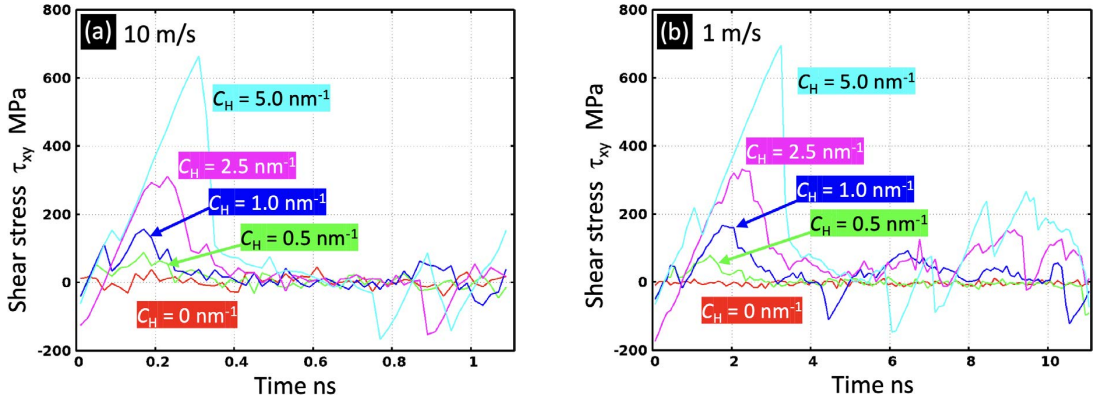

Fig. 2. The shear stress evolution at higher dislocation speeds at T = 300 K: (a) and (b) demonstrate the shear stress at V_d = 10 m/s and (a) V_d = 1 m/s, respectively. (Online version in color.)

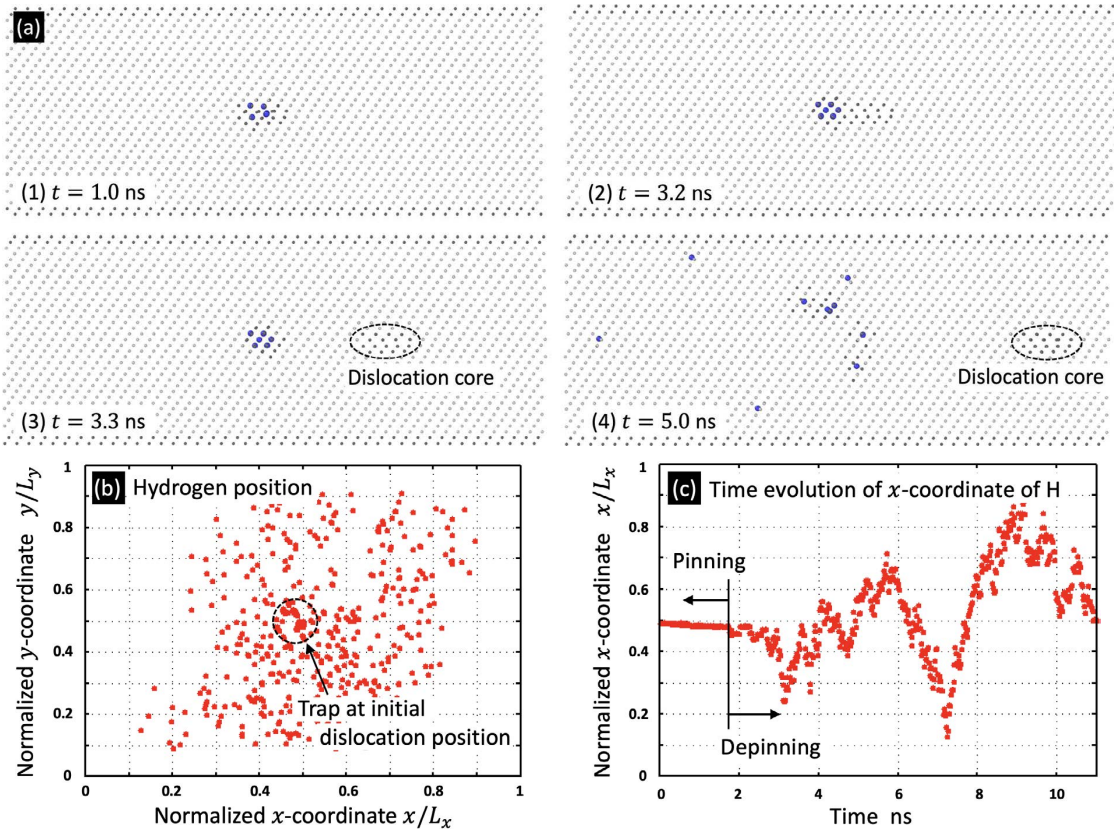

Fig. 3. Change of dislocation and hydrogen positions for V_d = 1 m/s and T = 300 K: (a) demonstrates the change of atomic arrange at (1) t = 1.0 ns, (2) t = 3.2 ns, (3) t = 3.3 ns, and (4) t = 5.0 ns for C_H = 5 nm^{-1}. The small light gray dots, small dark gray dots, and large blue dots represent Fe atoms composing bcc structure, Fe atoms composing non-bcc structure (defects), and H atoms, respectively. (b) demonstrates the hydrogen position in normalized coordinate by model size every 20 ps for C_H = 0.5 nm^{-1}. (c) demonstrates the evolution of the hydrogen atom's normalized x-coordinate. (Online version in color.)

the dislocation core moves forward, and hydrogen atoms are left behind with a sharp decrease in shear stress, as verified in Fig. 2 [Fig. 3(a)(3)]. The hydrogen atoms are finally released from the trapping by dislocation and diffuse away [Fig. 3(a)(4)]. The position of the hydrogen atom at the lowest hydrogen concentration (C_H = 0.5 nm^{-1}) and the evolution of the normalized x-coordinate (x/L_x) are demonstrated in Figs. 3(b) and 3(c), respectively. These figures also verify that the hydrogen atoms, which was trapped at the dislocation core started diffusing after the disjunction. This finding demonstrates the pinning of dislocation by hydrogen atoms and the depinning process at a high-speed migration of dislocation. The impact of the hydrogen concentration on the process was not observed.

Higher hydrogen concentration results in a higher peak value, and C_H = 5.0 nm^{-1} has a value higher than 600 MPa (Fig. 2). Here we observe that the hydrogen concentration C_H = 5.0 nm^{-1} correlates with the thermal equilibrium under a feeble hydrogen condition. By comparing with the yield stress of α-iron, this depinning process is challenging occurring in α-iron with a wide range of practical hydrogen conditions. If the applied shear stress on dislocation is lower than the depinning stress, the dislocation and hydrogen migrate together at a lower speed at the given stress, as explained in the following sections.

3.2. Hydrogen Effect at a Lower-Speed Migration

Figure 4 demonstrates the shear stress evolution at lower

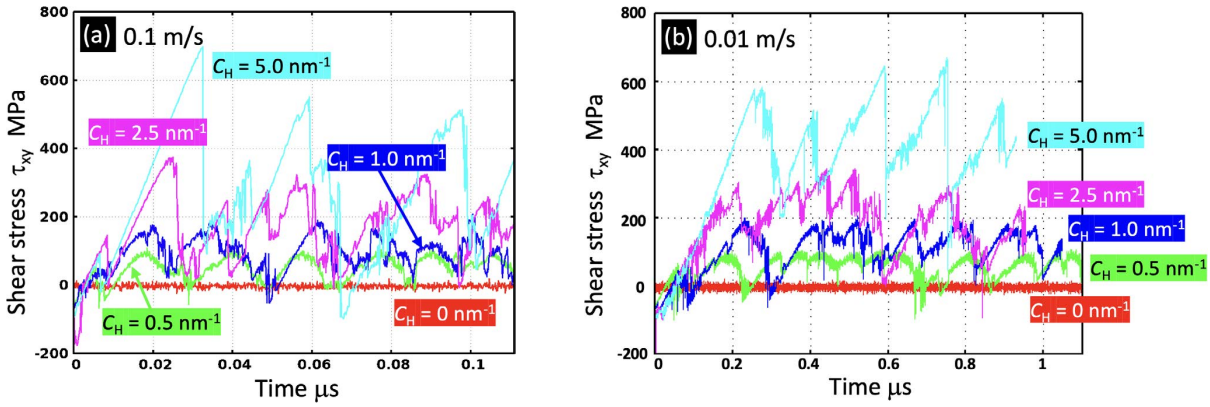

Fig. 4. The shear stress evolution at higher dislocation speeds at T = 300 K: (a) and (b) demonstrate the shear stress at V_d = 0.1 m/s and (a) V_d = 0.01 m/s, respectively. (Online version in color.)

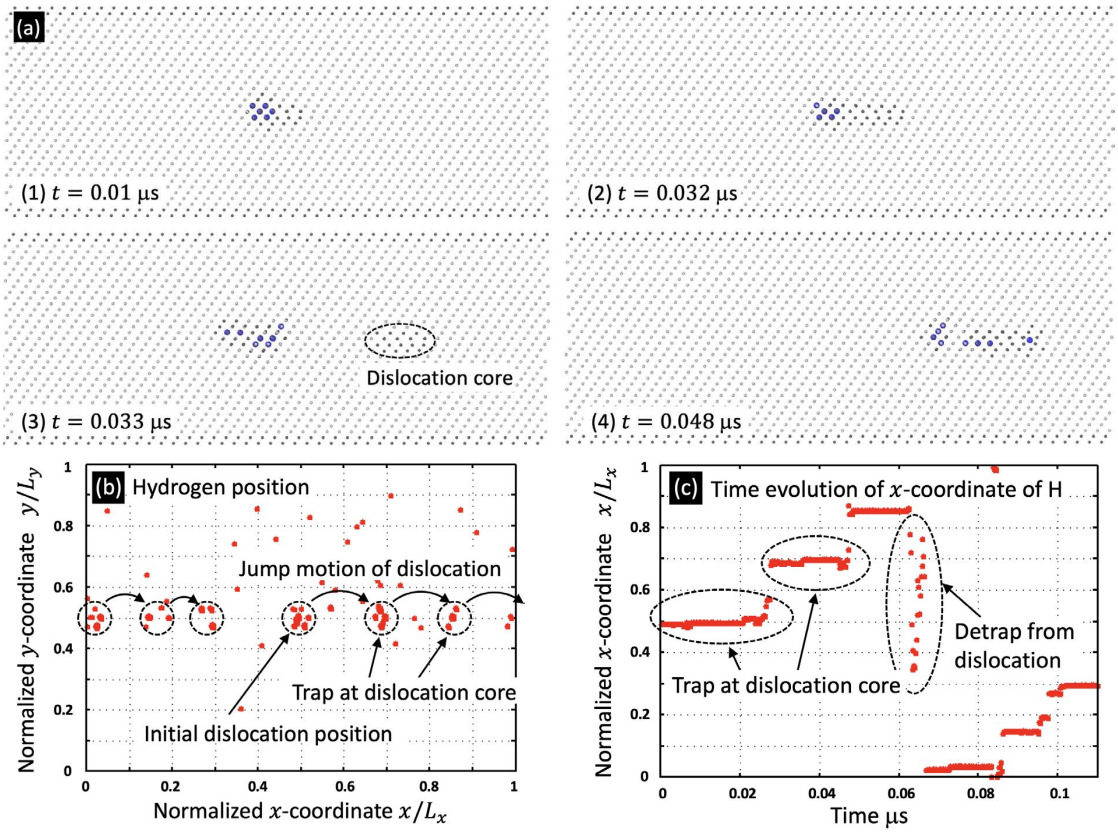

Fig. 5. Change of dislocation and hydrogen positions for V_d = 0.1 m/s and T = 300 K: (a) demonstrates the change of atomic arrange at (1) t = 0.01 μs, (2) t = 0.032 μs, (3) t = 0.033 μs, and (4) t = 0.048 μs for C_H = 5 nm^{-1}. (b) shows the hydrogen position in normalized coordinate every 200 ps for C_H = 0.5 nm^{-1}. (c) demonstrates the evolution of the hydrogen atom's normalized x-coordinate. (Online version in color.)

dislocation speeds (V_d = 0.1 and 0.01 m/s) at T = 300 K. In contrast to the higher dislocation velocity (Fig. 2), we could verify the jagged shape for all cases. The stress increases with increasing hydrogen concentration. At V_d = 0.1 m/s, the shear stress nearly reaches zero after reaching its peak and then increases again [Fig. 4(a)]. The magnitude of shear stress at each peak is almost the same as in the higher velocity cases (Fig. 2). The stress does not drop to zero after each peak at the slowest dislocation velocity (V_d = 0.01 m/s), [Fig. 4(b)]. Additionally, we can verify some steady periods with minor fluctuations in shear stress, such as 0.35–0.65 μs for C_H = 0.5 nm^{-1} and 0.3–0.5 μs for C_H = 2.5 nm^{-1}. The peak stress is slightly smaller compared with the higher velocity cases [Figs. 2 and 4(a)].

Figure 5 demonstrates the dislocation's positions and the hydrogen atoms when V_d = 0.1 m/s. Figure 5(a) demonstrates the structure change for the highest hydrogen concentration (C_H = 5 nm^{-1}). As demonstrated in Fig. 5(a), the positional relationship of hydrogen atoms and the dislocation core is identical to the higher dislocation speed [Figs. 3(a)(1)–(3) and 5(a)(1)–(3)] except for the last state [Figs. 3(a)(4) and 5(a)(4)]. For V_d = 0.1 m/s, although the depinning occurs with the stress drop and the dislocation's jump motion, the dislocation stays close to hydrogen atoms due to the slow motion, therefore, hydrogen atoms catch up with dislocation. This is due to the hydrogen diffusion along the slip direction being suppressed near the dislocation core by the uneven potential surface,[16,22] and the fast diffusion of hydrogen atoms recovers once they depart from the dislocation core. The hydrogen atoms catch up with the dislocation core by reaching through the upper or lower part of the simulation model. Figures 5(b) and 5(c) demonstrate the hydrogen position and the evolution of the normalized x-coordinate for the hydrogen concentration of C_H = 0.5 nm^{-1}, respectively. Further, we can verify the jerky motion of dislocation by the pinning, depinning, and retrapping of hydrogen. The findings were identical for all hydrogen concentrations.

The position of the dislocation and the hydrogen atoms for the slowest dislocation speed (V_d = 0.01 m/s) is depicted in **Fig. 6**. Figure 6(a) demonstrates the atomic structure every 0.05 μs for C_H = 5 nm^{-1}. The hydrogen atoms remain inside the dislocation core and completely follow the dislocation migration. In other words, the dislocation moves

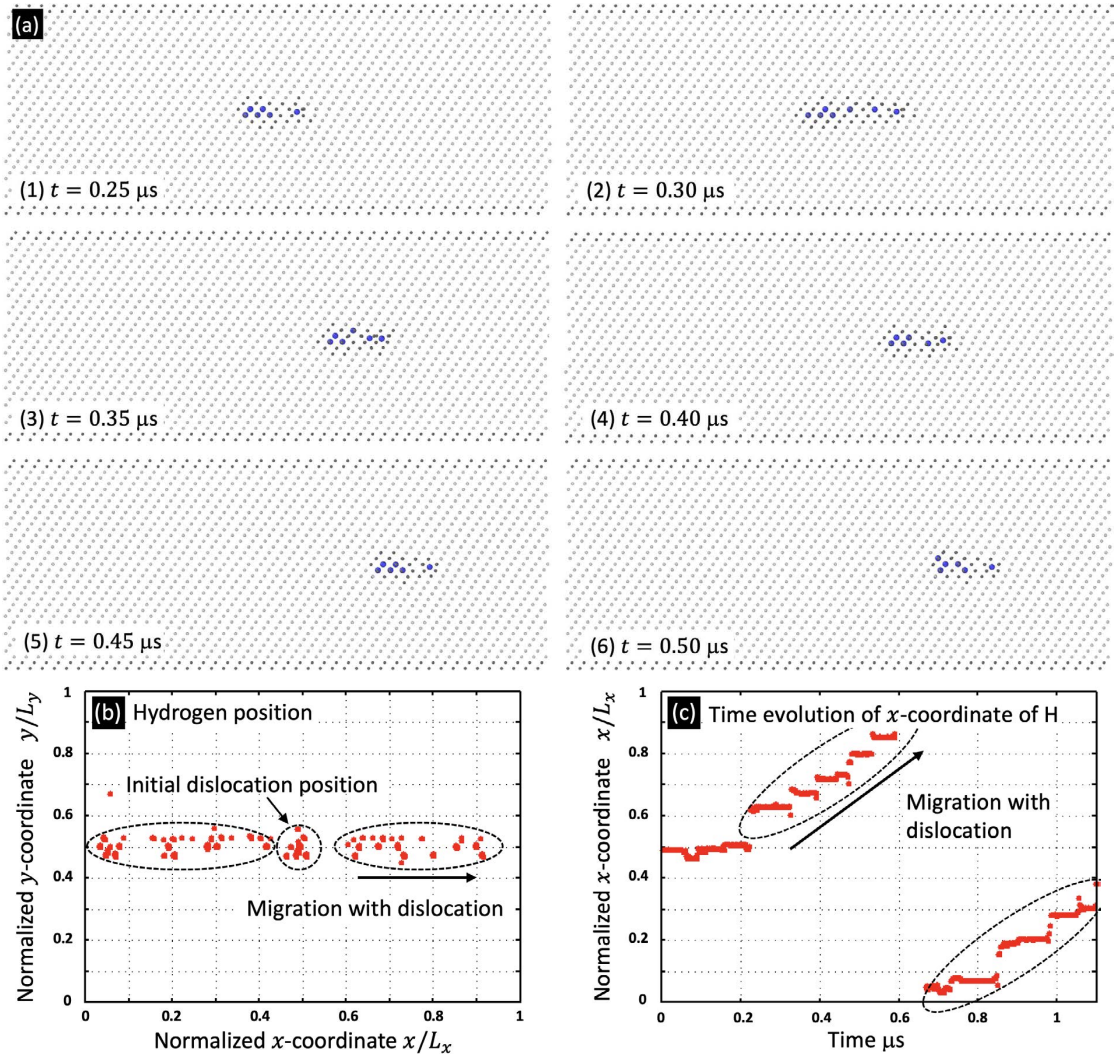

Fig. 6. Change of dislocation and hydrogen positions for V_d = 00.1 m/s and T = 300 K: (a) demonstrates the change of atomic arrange at (1) t = 0.25 μs, (2) t = 0.30 μs, (3) t = 0.35 μs, (4) t = 0.40 μs, (5) t = 0.45 μs, and (6) t = 0.048 μs for C_H = 5 nm^{-1}. (b) demonstrates the hydrogen position in normalized coordinate every 2 ns for C_H = 0.5 nm^{-1}. (c) demonstrates the evolution of the hydrogen atom's normalized x-coordinate. (Online version in color.)

with the hydrogen cloud's dragging. Figures 6(b) and 6(c) demonstrate the hydrogen position and the evolution of the hydrogen's normalized x-coordinate for a hydrogen concentration of $C_H = 0.5$ nm^{-1}, respectively. We can verify that the hydrogen atom follows the dislocation motion smoothly with small jumps in the core. The dragging motion of hydrogen by dislocation occurs at $V_d = 0.01$ m/s, and it was observed with the long timescale MD simulations over 1 μs. The averaged shear stress required to migrate the dislocation by dragging hydrogen at $V_d = 0.01$ m/s is demonstrated in **Table 2** together with the average stresses at the higher temperatures, which will be explained in Section 3.3. The averaged values were computed for $t >$ (0.2 nm)/V_d [s] to exclude the non-steady-state at the beginning. It is verified that very high stress (433 MPa for $C_H = 5$ nm^{-1}) is required to produce the dragging motion. Again, the hydrogen concentration along the dislocation core correlated with a very weak hydrogen condition. We consider that the jerky motion observed at $V_d = 0.1$ m/s (Fig. 5) corresponds to the transition phenomenon from the pinning of dislocation by hydrogen to the dragging of hydrogen by dislocation.

The previous static analysis employing the NEB approach demonstrated that the transition condition from pinning to dragging is ~25 m/s[10] (pinning at $\geq$ 50 m/s and dragging at $\leq$ 1.5 m/s) or the shear stress ~80 MPa at $C_H = 0.5$ nm^{-1} and 300 K. This analysis demonstrated it ~0.1 m/s (pinning at $\geq$ 1 m/s, jerky motion at 0.1 m/s, and dragging at $\leq$ 0.01 m/s) or ~100 MPa (the peak value in Fig. 4(a)) at the same hydrogen concentration. Although the prediction employing the NEB approach for a complicated phenomenon is challenging because of the challenge of finding all possible paths, the agreement is satisfactory. This analysis did not verify the improvement in dislocation mobility. Since the shear stress without hydrogen case is almost zero from the beginning for α-Iron, the verification is very challenging due to the thermal fluctuation of MD findings even if the effect occurs.

The quantum impact is crucial for the diffusion of hydrogen in α-iron lattice,[26] and the impact is not considered in the current analysis. However, since the distance between trap sites that substantially affects the quantum diffusion is prominent in the dislocation core, it is considered that the quantum diffusion impact does not modify the current finding.

Table 2. Temperature and dislocation speed effect on the average shear stress necessary to migrate the edge dislocation with hydrogen.

Temperature	Average shear stress [MPa] at different hydrogen concentrations [nm^{-1}] (Calculated stress using Eq. (1))			
	$C_H = 0.5$	$C_H = 1$	$C_H = 2.5$	$C_H = 5$
$V_d = 0.01$ m/s $T = 300$ K	57 (41)	124 (83)	196 (206)	433 (413)
$V_d = 0.01$ m/s T = 400 K	< 5 (5)	< 5 (10)	86 (26)	100 (52)
$V_d = 0.01$ m/s $T = 500$ K	< 5 (1)	< 5 (3)	< 5 (7)	8 (14)
$V_d = 0.1$ m/s $T = 400$ K	35 (40)	86 (81)	210 (202)	326 (403)
$V_d = 0.1$ m/s $T = 500$ K	10 (13)	24 (26)	74 (64)	136 (128)

3.3. Influence of Temperature and Prediction of Necessary Shear Stress at Lower Dislocation Speed

Figure 7 demonstrates the evolution of shear stress for higher temperatures ($T = 400$ K and $T = 500$ K) when $V_d = 0.01$ m/s. By increasing the temperature, the shear stress is significantly reduced. The average share stresses for higher temperatures are demonstrated in Table 2. The required stress is almost zero for lower concentrations at 400 K and all concentrations at 500 K. It is verified that the average shear stress is almost proportional to the hydrogen concentration C_H under the computed conditions (for example, if we compare the shear stress for $C_H = 0.5$ nm^{-1} and $C_H = 5$ nm^{-1}, the shear stress is almost 10 times.). **Figures 8**(a) and 8(b) respectively show the position of the hydrogen atom at $T = 400$ K and $T = 500$ K for $C_H = 0.5$ nm^{-1}. The hydrogen atom remains in the dislocation core and moves together at 400 K. Although the detrapping occasionally occurs because of the thermal effect, the hydrogen follows the dislocation motion at 500 K. We also verified that the hydrogen atom follows the dislocation core smoothly with small jumps when $V_d = 0.1$ m/s and $T = 500$ K, and the evolution of the hydrogen position at $V_d = 0.1$ m/s, $T = 400$ K is similar to $V_d = 0.01$ m/s, $T = 300$ K demonstrated in Fig. 5. The average stresses when dragging motion occurs

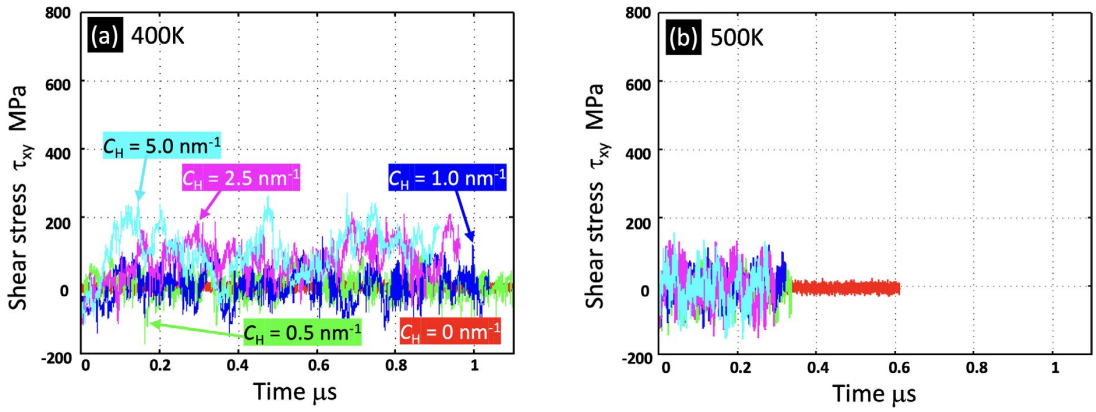

Fig. 7. The impact of temperature on the necessary shear stress to migrate dislocation when $V_d = 0.01$ m/s: (a) and (b) demonstrate the finding when $T = 400$ K and (b) $T = 500$ K, respectively. (Online version in color.)

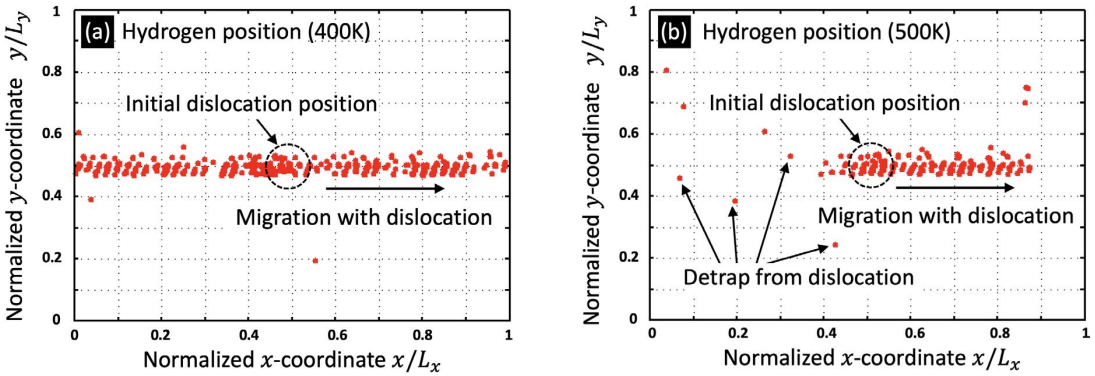

Fig. 8. Change of the hydrogen position for V_d = 00.1 m/s and C_H = 0.5 nm^{-1}: (a) and (b) demonstrate the hydrogen position in normalized coordinate every 2 ns for T = 400 K and T = 500 K, respectively. (Online version in color.)

are outlined in Table 2. We can verify that the dragging motion easily occurs at higher temperatures and lower hydrogen concentrations.

The simulation model employed here includes a relatively small number of atoms ($<10^4$ atoms), and the computation was conducted over a huge number of time steps (over 10 billion steps for H atoms). Parallel computing employing spatial decomposition is inefficient for such simulation, and therefore, decreasing the dislocation speed or increasing the timescale is quite challenging. Here, we postulate that the dislocation migration is controlled by the hydrogen diffusion in the dislocation core at a very low dislocation speed and moderate temperature. We also predict the required shear stress to migrate dislocation at lower speeds by employing the computed average stress (Table 2). Further, we propose that the dislocation speed is expressed by the stress-dependent thermal activation process based on the hydrogen diffusion rate-determining as follows.

$$V_d = \left(V_0 + V_{st}\tau^*\right)\left\{\exp\left(-\frac{\Delta E_0 - E_{st}\tau^*}{k_B T}\right) - \exp\left(-\frac{\Delta E_0 + E_{st}\tau^*}{k_B T}\right)\right\} \quad \text{.....(1)}$$

As a very rough assumption, we added the impact of hydrogen concentration along the dislocation line C_H in the stress effect in an inversely proportional manner as $\tau^* = \tau/C_H$, since the shear stress presented in Table 2 is almost proportional to C_H. The pre-factor ($V_0 + V_{st}\tau^*$) is a product of the vibrational frequency of hydrogen and the jump distance. Since the jump distance in the dislocation core varies depending on the dislocation speed and temperature as demonstrated in Figs. 6(b) and 8, we added the impact in the pre-factor as a linear function of shear stress as ($V_0 + V_{st}\tau^*$). Therefore, Eq. (1) phenomenologically includes the transitions of diffusion path at different temperatures and dislocation speeds as a function of shear stress. The brace's first and second terms express the hydrogen jump probability along with positive shear stress (rightward) and negative shear stress (leftward), respectively. V_0 is the pre-factor without shear stress, V_{st} gives the dependence of pre-factor on the shear stress and the hydrogen concentration along the dislocation line. ΔE_0 is the activation energy of hydrogen diffusion in the dislocation core without stress, and E_{st} is a parameter that expresses the shear stress and hydrogen concentration dependence of activation energy. k_B is the Bolzmann constant. We numerically fit the above equations to the values except for <5 MPa in Table 2, and we obtained $V_0 = 2.27 \times 10^4$ m/s, $V_{st} = 9.99 \times 10^4$ Pa^{-1}·s^{-1}, $\Delta E_0 = 0.271$ eV, and $E_{st} = 2.87 \times 10^{-22}$ m^2. The calculated value for V_0 is similar to the product of hydrogen vibration frequency ($\approx 10^{14}$ s^{-1}) and the jump distance ($\approx b$ = 0.248 nm), and calculated value for ΔE_0 is close to the activation energy of hydrogen in the dislocation core (0.26 eV).[10] By numerically solving Eq. (1) for the shear stress τ, we can predict the required shear stress at a given dislocation speed V_d, temperature T, and hydrogen concentration along the dislocation line C_H. The computed values from the fitted equation are also demonstrated in Table 2 in brackets. We can verify that, despite the simplified model, the equation reproduces reasonable values for most conditions including conditions with <5 MPa which were not used for the fitting process. The dependence of the required shear stress with dislocation speeds at a lower speed for C_H = 0.5 nm^{-1}, 5 nm^{-1}, and 150 nm^{-1} at T = 300 K are demonstrated in **Fig. 9**. It is verified that ≈ 100 MPa is required for C_H = 5 nm^{-1} even at V_d = 2 mm/s. If we extrapolate to C_H = 150 nm^{-1}, which is achieved at 70 MPa of gaseous hydrogen environment,[11] ≈ 100 MPa is required even at V_d = 60 μm/s. This finding shows that the edge dislocation migrates with a very slow speed (1 mm/s order or less) in the presence of hydrogen with the reason-

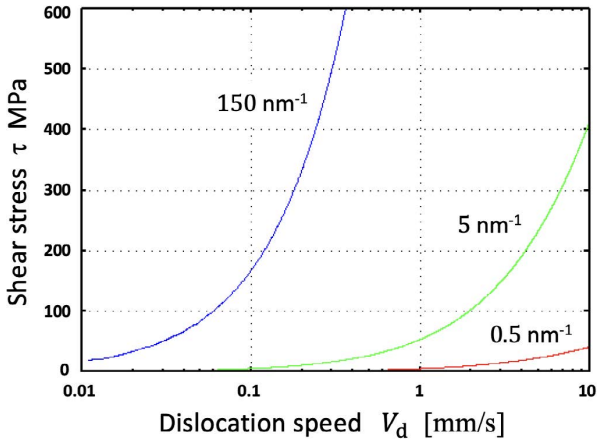

Fig. 9. The required shear stress at lower dislocation speed at T = 300 K: The predictions at different hydrogen concentrations along the dislocation line C_H = 0.5 nm^{-1}, 5 nm^{-1}, and 150 nm^{-1} are demonstrated. (Online version in color.)

able stress in α-iron.

In this research, only the hydrogen effect on the mobility of edge dislocation is examined. The motion of screw dislocation generally hinders the plastic deformation of α-iron, particularly at the later stage of deformation. However, the screw dislocation has a much smaller trap energy of hydrogen than edge dislocation.[21] It should be considered that when screw dislocation traps hydrogen, very high-density hydrogen exists around the edge dislocation due to the stronger trap energy. Recently, it has been experimentally observed that the density and proportion of screw dislocation increase when hydrogen is present.[27] The current analysis findings demonstrate that the screw dislocation activity requires to carry more deformation because the edge-dislocation motion is substantially reduced, and therefore the increases in screw-dislocation density[27] and flow-stress[7] are quite natural. The present results do not clarify how the screw-dislocation proportion changes, because the edge dilocation with reduced mobility can be stored in the lattice. However, the reduction of edge-dislocation mobility should impact the screw-dislocation proportion and the dislocation structure.

4. Conclusions

In this research, we conducted molecular dynamics (MD) simulations to analyze the hydrogen effect on edge dislocation motion at a wide range of dislocation speeds from 10 m/s to 0.01 m/s and a temperature range from 300 K to 500 K. The findings are outlined as follows.

(1) The movement of edge dislocations in α-Fe with hydrogen is significantly damped as the hydrogen concentration increases.

(2) The transition of the hydrogen effect on dislocation changes from pinning to dragging occurs at a dislocation speed of around 0.1 m/s at 300 K. When the dislocation velocity is reduced to 0.01 m/s, it is observed that hydrogen follows the edge-dislocation motion.

(3) The required stress to migrate the edge dislocation at 0.01 m/s is ~433 MPa, even at a low hydrogen concentration, which is achieved at a gaseous hydrogen environment with lower pressure than atmospheric pressure. The dragging motion of hydrogen by dislocation easily occurs at a higher temperature and a lower hydrogen concentration.

(4) The required shear stress at a lower dislocation speed was predicted by employing the stress-dependent thermal activation model. The finding demonstrated that the edge dislocation must slow down until 1 mm/s order or less in the presence of hydrogen to migrate with suitable shear stress in α-iron.

Acknowledgements

This research was supported by ISIJ Research Promotion Grant and JSPS KAKENHI Grant Number 19H02025.

REFERENCES

1) C. D. Beachem: *Metall. Trans.*, **3** (1972), 441. https://doi.org/10.1007/BF02642048
2) X.-Y. Liu, J. Kameda, J. W. Anderegg, S. Takaki, K. Abiko and C. J. McMahon, Jr.: *Mater. Sci. Eng. A*, **492** (2008), 218. https://doi.org/10.1016%2Fj.msea.2008.03.012
3) M. Nagumo: *Mater. Sci. Technol.*, **20** (2004), 940. https://doi.org/10.1179/026708304225019687
4) R. Matsumoto, S. Seki, S. Taketomi and N. Miyazaki: *Comput. Mater. Sci.*, **92** (2014), 362. https://doi.org/10.1016/j.commatsci.2014.05.029
5) T. Tabata and H. K. Birnbaum: *Scr. Metall.*, **17** (1983), 947. https://doi.org/10.1016/0036-9748(83)90268-5
6) P. Sofronis and H. K. Birnbaum: *J. Mech. Phys. Solids*, **43** (1995), 49. https://doi.org/10.1016/0022-5096(94)00056-B
7) Y. Sugiyama and K. Takai: *Acta Mater.*, **208** (2021), 116663. https://doi.org/10.1016/j.actamat.2021.116663
8) G. Henkelman and H. Jónsson: *J. Chem. Phys.*, **113** (2000), 9978. https://doi.org/10.1063/1.1323224
9) M. Itakura, H. Kaburaki, M. Yamaguchi and T. Okita: *Acta Mater.*, **61** (2013), 6857. https://doi.org/10.1016/j.actamat.2013.07.064
10) S. Taketomi, R. Matsumoto and N. Miyazaki: *J. Mater. Res.*, **26** (2011), 1269. https://doi.org/10.1557/jmr.2011.106
11) S. Taketomi, R. Matsumoto and S. Hagihara: *ISIJ Int.*, **57** (2017), 2058. https://doi.org/10.2355/isijinternational.ISIJINT-2017-172
12) J. Song and W. A. Curtin: *Acta Mater.*, **68** (2014), 61. https://doi.org/10.1016/j.actamat.2014.01.008
13) H. Yu, I. H. Katzarov, A. T. Paxton, A. C. F. Cocks and E. Tarleton: *Phys. Rev. Mater.*, **4** (2020), 033607. https://doi.org/10.1103/PhysRevMaterials.4.033607
14) R. Matsumoto and S. Taketomi: *Comput. Mater. Sci.*, **171** (2020), 109240. https://doi.org/10.1016/j.commatsci.2019.109240
15) R. Matsumoto, S. Taketomi, S. Matsumoto and N. Miyazaki: *Int. J. Hydrog. Energy*, **34** (2009), 9576. https://doi.org/10.1016/j.ijhydene.2009.09.052
16) S. Taketomi, R. Matsumoto and N. Miyazaki: *Acta Mater.*, **56** (2008), 3761. https://doi.org/10.1016/j.actamat.2008.04.011
17) M. Wen, X. J. Xu, S. Fukuyama and K. Yokogawa: *J. Mater. Res.*, **16** (2001), 3496. https://doi.org/10.1557/JMR.2001.0480
18) R. Matsumoto, Y. Inoue, S. Taketomi and N. Miyazaki: *Scr. Mater.*, **60** (2009), 555. https://doi.org/10.1016/j.scriptamat.2008.12.009
19) R. Matsumoto, N. Nishiguchi, S. Taketomi and N. Miyazaki: *J. Soc. Mater. Sci., Jpn.*, **63** (2014), 182. https://doi.org/10.2472/jsms.63.182
20) R. Matsumoto, M. Riku, S. Taketomi and N. Miyazaki: Progress in Nuclear Science and Technology, Vol. 2, Atomic Energy Society of Japan, Tokyo, (2011), 9. https://www.aesj.net/document/pnst002/009-015.pdf
21) S. Taketomi and R. Matsumoto: Handbook of Mechanics of Materials, Springer, Singapore, (2019), 283. https://doi.org/10.1007/978-981-10-6884-3_11
22) M. Tuckerman, B. J. Berne and G. J. Martyna: *J. Chem. Phys.*, **97** (1992), 1990. https://doi.org/10.1063/1.463137
23) S. Taketomi, R. Matsumoto and N. Miyazaki: *J. Mater. Sci.*, **43** (2008), 1166. https://doi.org/10.1007/s10853-007-2364-5
24) J. D. Honeycutt and H. C. Andersen: *J. Phys. Chem.*, **91** (1987), 4950. https://doi.org/10.1021/j100303a014
25) OVITO: OVITO Open Visualization Tool, https://www.ovito.org/, (accessed 2022-06-29).
26) S. Nagase and R. Matsumoto: *ISIJ Int.*, **61** (2021), 1294. https://doi.org/10.2355/isijinternational.ISIJINT-2020-340
27) K. Okada, A. Shibata, W. Gong and N. Tsuji: *Acta Mater.*, **225** (2022), 117549. https://doi.org/10.1016/j.actamat.2021.117549